Editors' Suggestion

Self-Trapping of Slow Electrons in the Energy Domain

Maor Eldar,[1,2,3] Zhaopin Chen,[1,2,3] Yiming Pan,[1,3,4] and Michael Krüger[1,2,3,*]
[1]Department of Physics, Technion—Israel Institute of Technology, Haifa 32000, Israel
[2]Solid State Institute, Technion—Israel Institute of Technology, Haifa 32000, Israel
[3]The Helen Diller Quantum Center, Technion—Israel Institute of Technology, Haifa 32000, Israel
[4]School of Physical Science and Technology and Center for Transformative Science, ShanghaiTech University, Shanghai 200031, China

(Received 29 September 2022; revised 22 September 2023; accepted 5 December 2023; published 17 January 2024)

The interaction of light and swift electrons has enabled phase-coherent manipulation and acceleration of electron wave packets. Here, we investigate this interaction in a new regime where low-energy electrons (∼20–200 eV) interact with a phase-matched light field. Our analytical and one-dimensional numerical study shows that slow electrons are subject to strong confinement in the energy domain due to the nonvanishing curvature of the electron dispersion. The spectral trap is tunable and an appropriate choice of light field parameters can reduce the interaction dynamics to only two energy states. The capacity to trap electrons expands the scope of electron beam physics, free-electron quantum optics and quantum simulators.

DOI: 10.1103/PhysRevLett.132.035001

The interaction between free electrons and light, resulting in a high degree of coherent control of the electron wave function, has been intensively studied during the past two decades [1–6]. While energy-momentum conservation in this interaction cannot be fulfilled in free space, introducing a third medium or body allows for the exchange of energy between photons and electrons. This can be achieved using different approaches, such as photon-induced near-field electron microscopy (PINEM, [1,4,7]), optical field discontinuities at interfaces [3,8], dielectric laser acceleration (DLA, [9–11]), flat surfaces with phase-matched near fields [5,12], photonic cavities [6,13], or ponderomotive acceleration [14–16]. The main signature of the interaction is the appearance of sidebands in the electron energy spectrum that are spaced by photon energy quanta of the driving light as a result of energy and momentum transfer between electrons and light (see, e.g., [1,4,11,16,17]). The sidebands enable attosecond electron pulses [8,18–23]. All these works have employed fast electrons (10–200 keV), enabling a straightforward understanding of much of the physics, primarily in the simplified picture of multilevel Rabi oscillations [4]. Here, the interaction with the optical field allows the electron to perform a quantum random walk on an infinite energy ladder. The multilevel Rabi oscillations model is based on approximations for fast electrons which include neglecting the electron momentum recoil (nonrecoil approximation), applying the short-time interaction approximation without phase matching, and neglecting the ponderomotive forces exerted by the strong light field. However, recent theory works have begun focusing on strong-field slow-electron interactions, for example via numerical study of strong off-resonant coupling at ∼0.1–1 keV [24], inelastic ponderomotive scattering at ∼10 keV [25], and Jaynes-Cummings-type interactions with a cavity [26]. Recent advancements in low-energy electron microscopy and source development have enabled the generation of tailored low-energy electron pulses [27–37], opening up first experimental studies of electron-light interactions in this novel regime.

In this Letter, we perform a theory study of the phase-matched interaction of slow electrons (∼20–200 eV) with a strong optical field. We find that resonant interactions in this regime cause a strong confinement of the low-energy electron spectrum due to the nonvanishing curvature of the electron dispersion. The latter acts as a quadratic trapping potential in the energy domain, setting a limit to the quantum random walk of the electrons. We show that this trapping in the energy domain is tunable due to the competition of energy ladder hopping and electron dispersion which depends strongly on the frequency and strength of the optical driving field. Our findings demonstrate that the rich toolbox for manipulating free electrons with light is not restricted to fast electrons, but gives rise to interesting new phenomena in the regime of low-energy electrons, much beyond the multilevel Rabi picture.

In order to understand the strong-field dynamics of slow electrons, we perform a Floquet-Bloch analysis of the

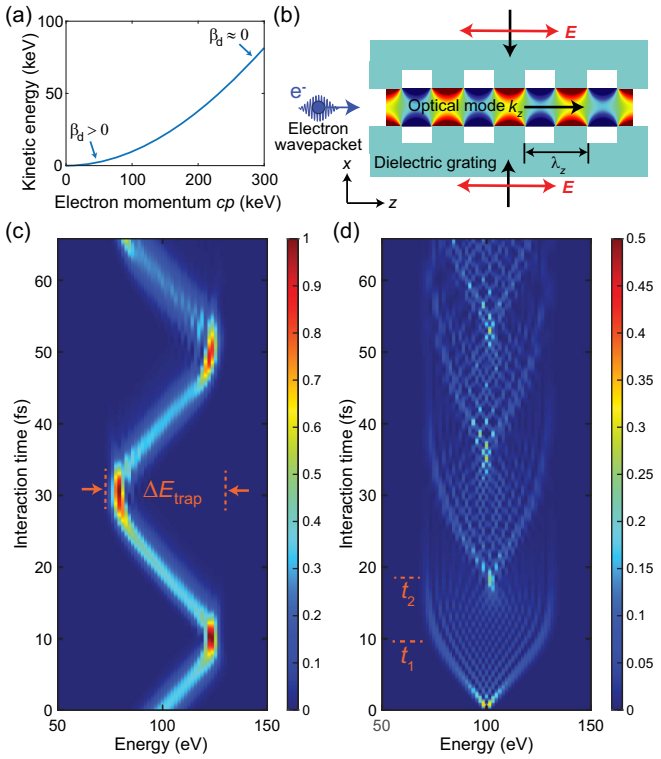

FIG. 1. Phase-matched low-energy electron light-matter interactions. (a) The electron dispersion for low-energy electrons displays a strong curvature β_d. (b) Sketch of a possible experimental setup. An electron is entering into a region of interaction with a phase-matched optical mode with wave vector k_z. Phase matching is achieved via a mirror-symmetric pair of dielectric gratings with a period of λ_z illuminated from both sides. (c) Evolution of the electron spectrum as a function of interaction time, as obtained from Eq. (1). The initial state is a localized wave packet with an energy width corresponding to five photons $\Delta E \sim 7.5$ eV (438 as temporal duration). The dashed lines represent the trap edges and the trap width ΔE_{trap}. (d) The same for a plane wave. In (c) and (d), the initial kinetic energy is set to $E_0 = 100$ eV. The optical field amplitude is $E_f = 0.5\,\mathrm{V\,nm^{-1}}$, the photon energy is $\hbar\omega = 1.54$ eV, and the phase is $\phi_0 = 0$.

time-dependent Schrödinger equation (TDSE). We reduce the problem to one spatial dimension along the electron's propagation direction (see Supplemental Material [38] for a full derivation and justification of this reduction). Key to our analysis is the electron's Hamiltonian given by $H_0 = E_0 + v_0(p - p_0) + (p - p_0)^2/(2\gamma^3 m)$, which we retrieve from expanding the relativistic dispersion to second order around the initial electron momentum p_0. The full relativistic dispersion is illustrated in Fig. 1(a). It displays a nonvanishing curvature β_d for low energies, which necessitates the second-order expansion for H_0. Here, m is the electron rest mass and $E_0 = \sqrt{m^2c^4 + p_0^2c^2} - mc^2$, $p_0 = \gamma m v_0$ and v_0 are the initial kinetic energy, momentum, and velocity, respectively, of the electron, while γ is the Lorentz factor and c the speed of light. In our proposed setup, we assume an optical mode with wave vector k_z, where k_z can be chosen such that a phase-matched electron-light interaction is achieved. An example of this is an evanescent mode induced at a DLA-type double grating structure with period λ_z [10], where $k_z = 2\pi/\lambda_z$ [see Fig. 1(b) and Supplemental Material [38] for a detailed discussion]. We neglect other modes in our theory study since they cannot lead to a net modulation of the electron. The interaction Hamiltonian is given by $H_I = -(e/2\gamma m)(Ap + pA) + (e^2A^2/2\gamma m)$, where A is the optical field's vector potential and e the elementary charge. For a monochromatic field, the vector potential is given by $A(z,t) = -(E_f/\omega)\sin(\omega t - k_z z + \phi_0)$, where E_f and ω are the electric field amplitude and angular frequency, respectively. ϕ_0 is the initial phase of the electric field at the beginning of the interaction ($t = 0$).

The electron-light interaction is imprinted on the resulting energy spectrum. After the electron enters the interaction region where the optical field is present it absorbs or emits an integer number of photons from the field, resulting in equally spaced energy states. Hence, encapsulating this spatiotemporal periodicity we employ the Floquet-Bloch ansatz $|\psi(t)\rangle = \sum_{n=-\infty}^{\infty} a_n(t)e^{-i\omega_n t}|k_n\rangle$, where n denotes the number of photons absorbed ($n > 0$) or emitted ($n < 0$) and a_n are the probability amplitudes corresponding to the respective energy-momentum states $|k_n\rangle$. Here, $k_n = k_0 + nk_z$ and $\omega_n = \omega_0 + n\omega$ denote the wave number and angular frequency values, respectively. The electron's initial kinetic energy and momentum are given by $\hbar\omega_0 \equiv (\gamma - 1)mc^2$ and $\hbar k_0 \equiv \gamma m v_0$, respectively. Substituting the ansatz into the Schrödinger equation we find

$$
\begin{aligned}
i\hbar\frac{\partial a_n(t)}{\partial t} = &-\left[n\hbar(\omega - v_0 k_z) - n^2\frac{(\hbar k_z)^2}{2m} + U_p\right]a_n(t) \\
&+ \delta\left(\left(k_{n+1} - \frac{k_z}{2}\right)a_{n+1}(t)e^{i\phi}\right. \\
&\left. + \left(k_{n-1} + \frac{k_z}{2}\right)a_{n-1}(t)e^{-i\phi}\right) \\
&- \frac{U_p}{2}\left(a_{n+2}(t)e^{i2\phi_0} + a_{n-2}(t)e^{-i2\phi_0}\right), \qquad (1)
\end{aligned}
$$

where $U_p = e^2E_f^2/(4m\omega^2)$ is the ponderomotive energy, $\delta = e\hbar E_f/(2m\omega)$ and $\phi = \phi_0 + (\pi/2)$. Equation (1) reveals several intriguing and unique characteristics of the slow electron-light interaction, as we will explain below.

In order to resonantly couple the slow electron and the field, we require the conservation of both energy and momentum for single photon emission or absorption by the electron at the quantum level, resulting in the phase-matching condition of equal electron (group) velocity and optical field (phase) velocity [42]. This phase-matching condition also holds true for low-energy electrons (see Supplemental Material [38]). In a DLA realization of our scheme using a grating, phase matching requires setting the grating period in accordance with the electron velocity

($v = \beta c$) and the impinging field's wavelength λ_f, namely $\lambda_z = \beta\lambda_f$ [9]. We note that it is challenging to achieve phase matching for slow electrons ($E_0 \approx 100$ eV) since it requires a significant reduction of the phase velocity of the optical field, but it is not impossible. For instance, DLA requires a grating structure with a period $\lambda_z \sim 16$ nm for 100 eV electrons and 800 nm free-space light wavelength, which is in reach of today's technological capabilities. As an alternative to DLA-type gratings, the use of plasmonic metamaterials [43] or materials with very high refractive index ($n \approx 50$), such as $SrTiO_3$ at low temperatures (~10 K, experimentally realized in [44]), can generate evanescent waves with an extremely small phase velocity. A prism configuration incorporating such materials enables phase-matched interactions [17]. Laser-triggered needle tips [27–36] produce suitable electron pulses with tunable bandwidth [32].

The A^2 ponderomotive term of the interaction Hamiltonian is reflected in the third line of Eq. (1), permitting two-photon exchanges in each interaction event. It becomes more important for slow electrons since the competing linear interaction term pA decreases with velocity. However, even for a 50 eV electron, strong electric fields with amplitudes on the order of 10 V nm^{-1} have to be applied to make the ponderomotive term comparable to the pA term. In contrast to free-space ponderomotive schemes [14,25,45], material damage thresholds limit the applicable field intensity. Under this limitation, a strong ponderomotive effect can still be reached if the electron kinetic energy approaches the single photon energy, $eE_f/\omega \approx p_0$ (see Supplemental Material [38]).

The second characteristic of slow-electron strong-field interaction is the breakdown of the nonrecoil approximation. For fast electrons, the detuning in momentum recoil owing to photon absorption and emission may be neglected, as explicitly represented by $k_{n+1} \approx k_{n-1} \approx k_0$ [4]. However, this is no longer true for slow electrons. In order to reveal this, we focus on the ratio $|\Delta v|/v_0$, where Δv is the velocity change caused by a single photon exchange. This quantity does not depend on the field strength. For an electron with $E_0 = 50$ eV and a photon energy $\hbar\omega = 1.54$ eV, we find $|\Delta v|/v_0 = \sqrt{\hbar\omega/E_0} \approx 10^{-1}$. In contrast, for a fast electron of $E_0 = 200$ keV we find $|\Delta v|/v_0 \approx 10^{-3}$, hence the detuning can be neglected. The breakdown of the nonrecoil approximation amounts to an effective symmetry breaking between absorption and emission, which is most pronounced at higher orders of photon scattering and manifests as a slightly altered coupling constant at the level of single photon exchange. In addition, we find an asymmetric evolution pattern in the electron spectrum when electrons and light are not phase matched. This leads to a different group velocity dispersion for emission and absorption sidebands, resulting in asymmetric Bloch-type oscillations (see Supplemental Material [38]).

The first line of Eq. (1) reveals two potentials acting on the time evolution of the sideband momentum states, $n\hbar(\omega - v_0 k_z)$ and $-(n\hbar k_z)^2/(2m)$. The first potential term is linear in n and results from the mismatch between electron group velocity and light field phase velocity. Under the condition $\omega \neq v_0 k_z$, this phase mismatch acts effectively as a linear potential on a synthetic frequency space resulting in Bloch oscillation dynamics in the energy spectrum as reported previously for fast free electrons [46,47], which lead to Wannier-Stark localization [48]. However, when we introduce phase matching through $\omega = v_0 k_z$, the linear term vanishes and we are left with the quadratic potential term. The latter is only significant for slow electrons and acts as a confining potential for the electron's spectral evolution. Figures 1(c) and 1(d) display the population probability of the sideband momentum states as function of interaction time obtained from numerical solutions of Eq. (1). We show the results for two initial conditions, a localized Gaussian wave packet [Fig. 1(c)] and a single energy [plane wave, Fig. 1(d)], both centered at 100 eV initial kinetic energy. The field strength is set to $E_f = 0.5$ V nm^{-1} and the single photon energy is $\hbar\omega = 1.54$ eV. We observe a spectral evolution exhibiting strong confinement and oscillations. For the electron wave packet, we find that the spectral evolution follows a classical Lorentz-like trajectory for a charged particle in an electric field. In contrast, for a plane-wave electron we see spectral broadening to a superposition state, which subsequently ceases to expand and suddenly collapses to a single sideband. In both cases, we observe a spectral asymmetry in the energy spectrum as a small but noticeable difference ($\Delta n \approx 3$) between the maximally populated energy states of absorption and emission. This asymmetry is a signature of the nonvanishing curvature of the electron dispersion at low energies and accumulates across successive photon scattering events. The validity of the results of our Floquet-Bloch model given by Eq. (1) is confirmed by a numerical solution of the full TDSE (see Supplemental Material [38]).

In order to analytically capture the basic underlying physics in Fig. 1, we lay aside the asymmetry in absorption and emission by applying the approximation $k_{n+1} \approx k_{n-1} \approx k_0$ and neglect ponderomotive effects. We are thus left with a simplified equation,

$$i\hbar \frac{\partial a_n}{\partial t} = \beta_d n^2 a_n + \kappa a_{n+1} + \kappa^* a_{n-1}, \tag{2}$$

where $\beta_d = ((\hbar k_z)^2/2m)$ and $\kappa = (eE_f\hbar k_0/2m\omega)e^{i(\phi_0+\pi/2)}$. By relating β_d to the electron and light field parameters under phase matching, we find $\beta_d \approx \frac{1}{4}(\hbar\omega)^2/E_0$. From Eq. (2) we can easily read the two competing processes that govern the spectral dynamics, namely harmonic oscillations and hopping. In analogy to solid-state terminology, we refer to the two terms on the rhs of Eq. (2) as quadratic

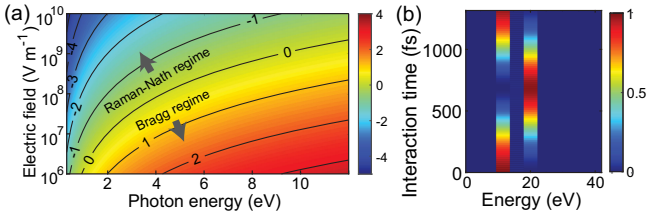

FIG. 2. (a) Transition between Raman-Nath and Bragg regimes. We show $\log\rho$ as a function of photon energy $\hbar\omega$ and electric field strength E_f. The initial electron energy is 100 eV. (b) Spectral evolution in the Bragg regime following Eq. (1) for an initial off-resonant electron energy of 12 eV, photon energy $\hbar\omega = 4$ eV, and $E_f = 1 \times 10^8$ V nm^{-1} ($\rho \approx 10$, $\lambda_z \sim 3$ nm for phase matching to 16 eV electron energy, which corresponds to $n = 0$). We observe Rabi-like oscillations between 12 eV ($n = -1$) and 20 eV ($n = +1$).

on-site potential ($n^2\beta_d$) and nearest-neighbor hopping (κ). Both parameters depend on the optical field parameters and the electron's energy dispersion. We note that the evolution of the electron spectrum governed by Eq. (2) is analogous to the Schrödinger equation for atomic diffraction [49], the transversal Kapitza-Dirac effect for electron diffraction [50] and acousto-optics (see Supplemental Material [38]). In order to distinguish the relative contribution of the two effects we invoke the Nath parameter, $\rho = \beta_d/\kappa$ [51]. In Fig. 2(a), we show $\log\rho$ as a function of photon energy and field strength. For $\rho \ll 1$, the hopping dominates, indicating the Raman-Nath regime, whereas for $\rho \gg 1$ we find the Bragg regime [52]. In the following, we will discuss both regimes and their effects on electron spectral evolution.

We first discuss the Raman-Nath regime ($\rho \ll 1$) which is reached when the hopping energy is much larger than the on-site energy. We can thus treat the latter as a perturbation. For instance, a slow electron with kinetic energy of 100 eV can reach this regime while interacting with an electric field with wavelength 800 nm and $E_f = 1$ V nm^{-1}, yielding $\rho \sim 10^{-3}$. The unperturbed equation then reads $i\hbar(\partial a_n(t)/\partial t) = \kappa a_{n+1}(t) + \kappa^* a_{n-1}(t)$, which has a known analytical solution in the form of a Bessel function of the first kind, $a_n(t) = J_n((2|\kappa|/i\hbar)t)e^{in\phi_0}$ (see Supplemental Material [38]). We obtain the probability $P_n(t)$ of locating the electron at a certain sideband as $P_n(t) = |J_n((2|\kappa|/i\hbar)t)|^2$. The quantum coherent dynamics given by the Bessel function solution entail a symmetric diffraction pattern, as observed in Fig. 1(d) for times smaller than $t_1 \sim 9$ fs, in full analogy to PINEM with fast electrons [4]. However, at later times, up to $t_2 \sim 19$ fs, the rapid expansion is considerably slowed down as the confining term ($\propto n^2$) becomes significant at these high sidebands. Physically, this is the result of energy–momentum conservation being violated at high photon scattering orders, due to the growing phase mismatch between light (linear dispersion) and free electron (quadratic dispersion). As a result, all electron trajectories are deflected from the trap edges and self-collapse in close vicinity of the initial momentum state at around $t_2 \sim 19$ fs, creating complex interference structures. This evolution pattern then repeats periodically throughout the interaction time due to the quadratic on-site potential.

For $\rho \gg 1$ where the hopping is smaller than the on-site potential term, we find the Bragg regime [50]. As shown in Fig. 2(a), entering the Bragg regime necessitates relatively weak electric fields ($\sim 10^6$–10^8 V m^{-1}) and high-energy photons ($\hbar\omega \sim 4$–20 eV). In this regime, fewer sideband orders are populated compared to the Raman-Nath regime, which can be understood as the quantum electron optics analog of optical Bragg diffraction but occurring here in the electron spectrum. The on-site term $\propto n^2$ invokes a symmetry between photon emission and absorption scattering orders $(n, -n)$. Therefore, even with a small hopping term of the Bragg regime, there exists a non-negligible coupling between these sidebands. For an initial spectrum containing only a single sideband, the Bragg regime can offer the strongest possible confinement involving only two sidebands, i.e., a coherent splitting of the electron spectrum much like a diffraction grating in optics. The dynamics takes the form of periodic oscillation between the two energy components, an effect known in neutron diffraction as Pendellösung oscillations [53], and was also observed in atom optics experiments [54]. A pure quantum effect occurs if the photon energy is on the order of the electron energy. Here, the slow electron populates only a few sidebands within a strong spectral confinement. The quantization grid in the electron phase space is comparable to its volume, therefore already exchanging a small number of photons leads to a large energy-momentum violation (large phase mismatch) and therefore eliminates higher sidebands [see Fig. 2(b) for an example]. Interestingly, for free-electron lasers a similar transition to a quantum regime was found [55]. We note that the truncation down to a two-level system with Rabi-like oscillations is only possible in the phase-matched Bragg regime and cannot be reached by other means, such as strong phase mismatch [46] or ponderomotive schemes [15,25] (see Supplemental Material [38]).

At this moment, we can control and manipulate the spectral confinement of the laser-modulated free electrons, enabling their trapping in the energy domain. This is achievable because the preceding analysis clarifies both the electron and light field parameters in each regime, as we will now demonstrate in detail. From now on throughout our Letter we stay in the Raman-Nath regime ($E_f \approx 1$V nm^{-1} and $\hbar\omega = 1.54$ eV). For our spectral trap, it is reasonable to define an effective trap width ΔE_{trap} as the energy difference between the minimum and the maximum populated sidebands [see Fig. 1(c)]. Large widths ΔE_{trap} correspond to weak trapping, whereas narrow ΔE_{trap} allow only a small number of sidebands to be populated. ΔE_{trap} stays the same for long interaction times and only depends on the field parameters and the initial electron energy distribution. In Fig. 3(a), we show the dependence of ΔE_{trap} on the electron

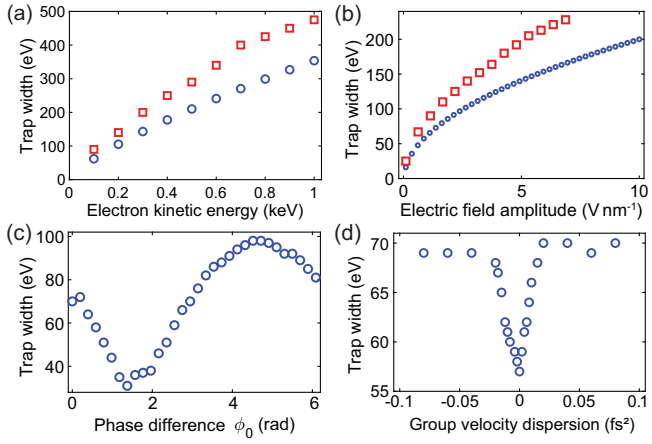

FIG. 3. Parameter dependence of the trap width. (a) Dependence on electron energy for $E_f = 1\ \mathrm{V\,nm^{-1}}$, $\hbar\omega = 1.54$ eV, and $\phi_0 = 0$. The phase matching is adjusted for each energy. Blue circles: initial wave packet as in Fig. 1(c). Red squares: plane wave. (b) The same as (a), but as a function of electric field amplitude for 100 eV electrons. (c) Dependence of the trap width on the relative phase between electron and light field for the wave packet. (d) Dependence on the group velocity dispersion of the wave packet, $\phi_0 = 0$.

energy for the wave packet and the plane wave from Figs. 1(c) and 1(d), respectively, with the phase matching adjusted to each energy. Not surprisingly, an increase in energy leads to weaker influence of the quadratic potential and therefore weaker trapping. A similar increase in width is reached by increasing the optical field strength, which enhances the hopping [see Fig. 3(b)]. The definition of κ reveals another parameter that influences the trap width, the phase ϕ_0 of the optical field at $t = 0$. This dependence can be explained with an analogy to the classical harmonic oscillator, for which the largest energy transfer between the driving force and mass occurs when the phase difference (time difference) between the two is $(\pi/2)$. In our definitions, this phase difference corresponds to $\phi_0 = (3\pi/2)$, where we indeed find the maximum ΔE_{trap} [see Fig. 3(c)]. Figure 3(d) shows the dependence of ΔE_{trap} on the group velocity dispersion (GVD) of the electron wave packet for $\phi_0 = 0$. As we move away from zero GVD, the trap width is increasing as the initial wave packet stretches in time and starts to resemble a continuous wave packet (see Supplemental Material [38] for details). We note that spectral trapping can also occur for larger electron energies than those treated in this Letter. However, the trap width will be on the order of the electron energy, making the effect hard to observe (see Supplemental Material [38]).

In Fig. 1(c), we notice the appearance of spectral Airy-like fringes forming at intermediate and long evolution times in the vicinity of the trap edges, i.e., at the turning points for a confined and oscillatory localized wave packet. These fringes are due to an interference pattern which emerges from the different phases accumulated by the set of initially occupied sideband states. The difference in phase accumulation by the different plane waves is strongest in the vicinity of the trap edges. A few oscillation cycles are required to develop a pronounced fringe pattern. This may be demonstrated by initializing the wave packet closer to the quadratic potential minimum by altering the phase difference, which results in longer interaction times for the fringes to form and vice versa.

In conclusion, our Letter explores the spectral dynamics of the resonant interaction of a low-energy electron with a strong light field. With the help of analytical models and numerical simulations, we find new spectral features appearing as the interaction evolves. Particularly, we report a confinement of the electron spectrum induced by the curvature of the electron dispersion which is not accessible for fast electrons. Tunable with the help of the optical field parameters, effective trap widths ranging from a few tens to a few hundred electron volts can be achieved. Our findings can be highly useful for quantum coherent electron manipulation. First, a confinement to only a few energy sidebands in the Bragg regime offers a natural truncation of the infinite Hilbert space of the multilevel Rabi ladder, allowing for adiabatic eliminations that enable us to get rid of undesired sidebands and higher-order photon transitions. Second, the finite Hilbert space as a synthetic spatial dimension can be then of aid for carrying out quantum simulations and computations utilizing coherent laser-electron interactions, as proposed recently for fast electrons [47]. Finally, the dynamical confinement in the low-energy regime can help to control the maximum energy transfer for laser-driven charged-particle acceleration, the minimum bunching size of an electron beam, and the maximum photon energy produced in free-electron radiation.

The authors acknowledge Martin Kozák, Bin Zhang, Ido Kaminer, and Peter Hommelhoff for useful discussions. This project has received funding from the European Union's Horizon 2020 research and innovation program under Grant Agreement No. 853393-ERC-ATTIDA. We also acknowledge the Helen Diller Quantum Center at the Technion for partial financial support.

*Corresponding author: krueger@technion.ac.il

[1] B. Barwick, D. J. Flannigan, and A. H. Zewail, Photon-induced near-field electron microscopy, Nature (London) **462**, 902 (2009).

[2] F. J. García de Abajo, Optical excitations in electron microscopy, Rev. Mod. Phys. **82**, 209 (2010).

[3] F. O. Kirchner, A. Gliserin, F. Krausz, and P. Baum, Laser streaking of free electrons at 25 keV, Nat. Photonics **8**, 52 (2014).

[4] A. Feist, K. E. Echternkamp, J. Schauss, S. V. Yalunin, S. Schäfer, and C. Ropers, Quantum coherent optical phase modulation in an ultrafast transmission electron microscope, Nature (London) **521**, 200 (2015).

[5] R. Dahan, S. Nehemia, M. Shentcis, O. Reinhardt, Y. Adiv, X. Shi, O. Be'er, M. H. Lynch, Y. Kurman, K. Wang, and I. Kaminer, Resonant phase-matching between a light wave and a free-electron wavefunction, Nat. Phys. **16**, 1123 (2020).
[6] J.-W. Henke, A. S. Raja, A. Feist, G. Huang, G. Arend, Y. Yang, F. J. Kappert, R. N. Wang, M. Möller, J. Pan, J. Liu, O. Kfir, C. Ropers, and T. J. Kippenberg, Integrated photonics enables continuous-beam electron phase modulation, Nature (London) **600**, 653 (2021).
[7] R. Shiloh, T. Chlouba, and P. Hommelhoff, Quantum-coherent light-electron interaction in a scanning electron microscope, Phys. Rev. Lett. **128**, 235301 (2022).
[8] Y. Morimoto and P. Baum, Diffraction and microscopy with attosecond electron pulse trains, Nat. Phys. **14**, 252 (2018).
[9] J. Breuer and P. Hommelhoff, Laser-based acceleration of nonrelativistic electrons at a dielectric structure, Phys. Rev. Lett. **111**, 134803 (2013).
[10] E. Peralta, K. Soong, R. J. England, E. R. Colby, Z. Wu, B. Montazeri, C. McGuinness, J. McNeur, K. J. Leedle, D. Walz, E. Sozer, B. Cowan, B. Schwartz, G. Travish, and R. L. Byer, Demonstration of electron acceleration in a laser-driven dielectric microstructure, Nature (London) **503**, 91 (2013).
[11] Y. Adiv, K. Wang, R. Dahan, P. Broaddus, Y. Miao, D. Black, K. Leedle, R. L. Byer, O. Solgaard, R. J. England, and I. Kaminer, Quantum nature of dielectric laser accelerators, Phys. Rev. X **11**, 041042 (2021).
[12] M. Kozák, P. Beck, H. Deng, J. McNeur, N. Schönenberger, C. Gaida, F. Stutzki, M. Gebhardt, J. Limpert, A. Ruehl, I. Hartl, O. Solgaard, J. S. Harris, R. L. Byer, and P. Hommelhoff, Acceleration of sub-relativistic electrons with an evanescent optical wave at a planar interface, Opt. Express **25**, 19195 (2017).
[13] O. Kfir, H. Lourenço-Martins, G. Storeck, M. Sivis, T. R. Harvey, T. J. Kippenberg, A. Feist, and C. Ropers, Controlling free electrons with optical whispering-gallery modes, Nature (London) **582**, 46 (2020).
[14] M. Kozák, T. Eckstein, N. Schönenberger, and P. Hommelhoff, Inelastic ponderomotive scattering of electrons at a high-intensity optical travelling wave in vacuum, Nat. Phys. **14**, 121 (2018).
[15] W. C.-W. Huang, H. Batelaan, and M. Arndt, Kapitza-Dirac blockade: A universal tool for the deterministic preparation of non-Gaussian oscillator states, Phys. Rev. Lett. **126**, 253601 (2021).
[16] M. Tsarev, J. W. Thurner, and P. Baum, Nonlinear-optical quantum control of free-electron matter waves, Nat. Phys. **19**, 1350 (2023).
[17] R. Dahan, A. Gorlach, U. Haeusler, A. Karnieli, O. Eyal, P. Yousefi, M. Segev, A. Arie, G. Eisenstein, P. Hommelhoff, and I. Kaminer, Imprinting the quantum statistics of photons on free electrons, Science **373**, eabj7128 (2021).
[18] K. E. Priebe, C. Rathje, S. V. Yalunin, T. Hohage, A. Feist, S. Schäfer, and C. Ropers, Attosecond electron pulse trains and quantum state reconstruction in ultrafast transmission electron microscopy, Nat. Photonics **11**, 793 (2017).
[19] M. Kozák, All-optical scheme for generation of isolated attosecond electron pulses, Phys. Rev. Lett. **123**, 203202 (2019).
[20] D. S. Black, U. Niedermayer, Y. Miao, Z. Zhao, O. Solgaard, R. L. Byer, and K. J. Leedle, Net acceleration and direct measurement of attosecond electron pulses in a silicon dielectric laser accelerator, Phys. Rev. Lett. **123**, 264802 (2019).
[21] N. Schönenberger, A. Mittelbach, P. Yousefi, J. McNeur, U. Niedermayer, and P. Hommelhoff, Generation and characterization of attosecond microbunched electron pulse trains via dielectric laser acceleration, Phys. Rev. Lett. **123**, 264803 (2019).
[22] Y. Morimoto and P. Baum, Single-cycle optical control of beam electrons, Phys. Rev. Lett. **125**, 193202 (2020).
[23] C. M. S. Sears, E. Colby, R. Ischebeck, C. McGuinness, J. Nelson, R. Noble, R. H. Siemann, J. Spencer, D. Walz, T. Plettner, and R. L. Byer, Production and characterization of attosecond electron bunch trains, Phys. Rev. Accel. Beams **11**, 061301 (2008).
[24] N. Talebi, Strong interaction of slow electrons with near-field light visited from first principles, Phys. Rev. Lett. **125**, 080401 (2020).
[25] M. Kozák and T. Ostatnický, Asynchronous inelastic scattering of electrons at the ponderomotive potential of optical waves, Phys. Rev. Lett. **129**, 024801 (2022).
[26] A. Karnieli and S. Fan, Jaynes-Cummings interaction between low-energy free electrons and cavity photons, Sci. Adv. **9**, eadh2425 (2023).
[27] P. Hommelhoff, Y. Sortais, A. Aghajani-Talesh, and M. A. Kasevich, Field emission tip as a nanometer source of free electron femtosecond pulses, Phys. Rev. Lett. **96**, 077401 (2006).
[28] C. Ropers, D. R. Solli, C. P. Schulz, C. Lienau, and T. Elsaesser, Localized multiphoton emission of femtosecond electron pulses from metal nanotips, Phys. Rev. Lett. **98**, 043907 (2007).
[29] B. Barwick, C. Corder, J. Strohaber, N. Chandler-Smith, C. Uiterwaal, and H. Batelaan, Laser-induced ultrafast electron emission from a field emission tip, New J. Phys. **9**, 142 (2007).
[30] M. Krüger, M. Schenk, and P. Hommelhoff, Attosecond control of electrons emitted from a nanoscale metal tip, Nature (London) **475**, 78 (2011).
[31] E. Quinonez, J. Handali, and B. Barwick, Femtosecond photoelectron point projection microscope, Rev. Sci. Instrum. **84**, 103710 (2013).
[32] L. Wimmer, G. Herink, D. R. Solli, S. V. Yalunin, K. E. Echternkamp, and C. Ropers, Terahertz control of nanotip photoemission, Nat. Phys. **10**, 432 (2014).
[33] D. Ehberger, J. Hammer, M. Eisele, M. Krüger, J. Noe, A. Högele, and P. Hommelhoff, Highly coherent electron beam from a laser-triggered tungsten needle tip, Phys. Rev. Lett. **114**, 227601 (2015).
[34] J. Vogelsang, G. Hergert, D. Wang, P. Groß, and C. Lienau, Observing charge separation in nanoantennas via ultrafast point-projection electron microscopy, Light Sci. Appl. **7**, 55 (2018).
[35] J. Vogelsang, N. Talebi, G. Hergert, A. Wöste, P. Groß, A. Hartschuh, and C. Lienau, Plasmonic-nanofocusing-based electron holography, ACS Photonics **5**, 3584 (2018).
[36] M. Krüger, C. Lemell, G. Wachter, J. Burgdörfer, and P. Hommelhoff, Attosecond physics phenomena at nanometric tips, J. Phys. B **51**, 172001 (2018).

[37] M. Eldar, S. Abo-Toame, and M. Krüger, Sub-optical-cycle electron pulse trains from metal nanotips, J. Phys. B **55**, 074001 (2022).
[38] See Supplemental Material at http://link.aps.org/supplemental/10.1103/PhysRevLett.132.035001 for complete derivations, supplemental discussions, and supplemental figures, which includes Refs. [39–41].
[39] J. Li, D. Zheng, S. Huang, J. Li, Y. Tian, Y. Zhang, Z. Li, H. Tian, and H. X. Yang, Efficiently accelerated free electrons by metallic laser accelerator, Nat. Commun. **14**, 5857 (2023).
[40] K. Soong, R. L. Byer, E. R. Colby, R. J. England, and E. A. Peralta, Laser damage threshold measurements of optical materials for direct laser accelerators, AIP Conf. Proc. **1507**, 511 (2012).
[41] A. Korpel, Acousto-optics—A review of fundamentals, Proc. IEEE **69**, 48 (1981).
[42] S. T. Park, M. Lin, and A. H. Zewail, Photon-induced near-field electron microscopy (PINEM): Theoretical and experimental, New J. Phys. **12**, 123028 (2010).
[43] K. L. Tsakmakidis, O. Hess, R. W. Boyd, and X. Zhang, Ultraslow waves on the nanoscale, Science **358**, eaan5196 (2017).
[44] T. Sakudo and H. Unoki, Dielectric properties of $SrTiO_3$ at low temperatures, Phys. Rev. Lett. **26**, 851 (1971).
[45] D. L. Freimund, K. Aflatooni, and H. Batelaan, Observation of the Kapitza-Dirac effect, Nature (London) **413**, 142 (2001).
[46] A. Pick, O. Reinhardt, Y. Plotnik, L. J. Wong, and I. Kaminer, Bloch oscillations of a free electron in a strong field, in *CLEO: QELS_Fundamental Science* (Optica Publishing Group, Washington DC, 2018), pp. FF1E–5.
[47] Y. Pan, B. Zhang, and D. Podolsky, Synthetic dimensions using ultrafast free electrons, arXiv:2207.07010.
[48] G. H. Wannier, Wave functions and effective Hamiltonian for Bloch electrons in an electric field, Phys. Rev. **117**, 432 (1960).
[49] P. Meystre and M. O. Scully, *Quantum optics* (Springer, New York, 2021).
[50] H. Batelaan, Colloquium: Illuminating the Kapitza-Dirac effect with electron matter optics, Rev. Mod. Phys. **79**, 929 (2007).
[51] N. N. Nath, The diffraction of light by supersonic waves, in Proc. Indian Acad. Sci. A **8**, 499 (1938).
[52] M. Moharam and L. Young, Criterion for Bragg and Raman-Nath diffraction regimes, Appl. Opt. **17**, 1757 (1978).
[53] C. G. Shull, Observation of Pendellösung fringe structure in neutron diffraction, Phys. Rev. Lett. **21**, 1585 (1968).
[54] P. J. Martin, B. G. Oldaker, A. H. Miklich, and D. E. Pritchard, Bragg scattering of atoms from a standing light wave, Phys. Rev. Lett. **60**, 515 (1988).
[55] P. Kling, E. Giese, R. Endrich, P. Preiss, R. Sauerbrey, and W. P. Schleich, What defines the quantum regime of the free-electron laser?, New J. Phys. **17**, 123019 (2015).